An Application of Remotely Derived Climatological Fields for Risk Assessment of Vector-Borne Diseases: A Spatial Study of Filariasis Prevalence in the Nile Delta, Egypt

M.K. Crombie, R.R. Gillies, R.E. Arvidson, P. Brookmeyer, G.J. Weil, M. Sultan, amd M. Harb

Abstract

This paper applies a relatively straightforward remote sensing method that is commonly used to derive climatological variables. Measurements of surface reflectance and surface radiant temperature derived from Landsat Thematic Mapper data were used to create maps of fractional vegetation and surface soil moisture availability for the southern Nile delta in Egypt. These climatological variables were subsequently used to investigate the spatial distribution of the vector borne disease Bancroftian filariasis in the Nile delta where it is focally endemic and a growing problem. Averaged surface soil moisture values, computed for a 5-km border area around affected villages, were compared to filariasis prevalence rates. Prevalence rates were found to be negligible below a critical soil moisture value of 0.2, presumably because of a lack of appropriate breeding sites for the Culex Pipiens mosquito species.

With appropriate modifications to account for local conditions and vector species, this approach should be useful as a means to map, predict, and control insect vector-borne diseases that critically depend on wet areas for propagation. This type of analysis may help governments and health agencies that are involved in filariasis control to better focus limited resources to identifiable "high-risk" areas.

Introduction

Bancroftian filariasis is a deforming illness transmitted by mosquitoes and caused by the parasite Wuchereria bancrofti (WHO, 1992; Neva and Brown, 1994) that affects approximately 120 million people in over 70 countries in tropical and subtropical regions worldwide (Ottesen and Ramachandran, 1995). The transmission of filariasis is strongly influenced by available moisture because the mosquito vector requires standing water for breeding and humid atmospheric conditions for the prolonged survival needed for transmission of the infection. Numerous studies have demonstrated the usefulness of remote sensing data in mapping environmental risk factors such as diurnal temperature variations and land-use practices that control, in part, the distribution of tropical diseases, including schistosomiasis, trypanosomiasis, and malaria (Rodgers and Randolph, 1991; Beck *et al.*, 1994; Malone *et al.*, 1994, Malone *et al.*, 1997).

Recent innovations (Gillies and Carlson, 1995; Kustas and Norman, 1996; Gillies *et al.*, 1997) in the use of true biophysical measurements (i.e., reflectance and radiant temperature measurements) of remotely sensed observations show how climatological variables (e.g., soil water content) over regional scales can be obtained by inversion; defined as fitting a measured variable to a simulated (modeled) one, such that their equivalence defines a solution. Such derived parameters can act as proxies for overall ambient atmospheric conditions (e.g., humidity) and help predict favorable environments for the development and transmission of filariasis. For example, in a recent study Thompson *et al.*, (1996) used Advanced Very High Resolution Radiometer (AVHRR) satellite data to map the diurnal temperature fluctuations (dT) of the Nile delta as a proxy for soil water content. Statistical comparison of filariasis prevalence and dT showed a good correlation between the median dT values of 10-square-kilometer areas and three filariasis prevalence level groupings (5, 15, and 25 percent). Their study, however, was limited by the course spatial resolution (1-km resolution at nadir) of the AVHRR sensor and the fact that such bulk surface temperature measurements can, by definition, only proxy soil moisture content in a very crude way, because the measurements do not account for the distribution of vegetation. Vegetation tends to maintain a constant radiative temperature during the day, providing that the plants are not water stressed (a reasonable assumption in an irrigated area like the Nile delta). Consequently, as fractional vegetation cover increases in any spatial domain, in this case an AVHRR pixel, the radiant temperature measurement from the vegetation increasingly modulates the pixel radiant temperature and, thereby, reflects less and less the actual soil surface moisture conditions.

In this study, higher spatial resolution remote sensing data

M.K. Crombie, R.E. Arvidson, and P. Brookmeyer are with the Department of Earth and Planetary Science, Washington University, St. Louis, MO 63130.

R.R. Gillies is with the Department of Soils, Plants and Biometeorology, Department of Geography and Earth Resources, Utah State University, Logan, UT 84322-4820.

G.J. Weill is with the Infectious Diseases Division, Department of Medicine, Washington University School of Medicine, St. Louis, MO 63130.

M. Sultan is with the Environmental Research Division, Argonne National Laboratory, Argonne, IL 60439.

M. Harb is with the Ministry of Health, Government of Egypt, Cairo, Egypt.

Photogrammetric Engineering & Remote Sensing
Vol. 65, No. 12, December 1999, pp. 1401–1409.

0099-1112/99/6512–1401$3.00/0

from Landsat TM 4 and 5, nominally 30-meter ground-projected instantaneous field of view (IFOV) in all bands except the thermal (120 m), from 1990 were used to calculate the available surface soil moisture, as opposed to a diurnal temperature variation, as an environmental risk factor for infection with Wuchereria bancrofti. The southern Nile delta of Egypt (Figure 1), where filariasis is focally endemic and re-emergent (Southgate, 1979; Feinsod, 1987; Harb, 1993), was chosen as the study site because of concurrency in available Landsat TM satellite coverage and filariasis prevalence data collected by the Egyptian Ministry of Health over the period 1985 to 1991 in 314 villages throughout the delta. One-hundred seventy-three villages located in the southern delta are considered in this study. Prevalence (Fisher and van Belle, 1993) is defined as

$$\text{Prevalence} = \frac{\text{Number of cases at a point in time in each village}}{\text{Population size of each village}}.$$

The prevalence data in this study represent point prevalence rates because villages were sampled on only one occasion. The surface soil moisture conditions were calculated using a technique developed by Gillies and Carlson (1995) that uses normalized radiant surface temperature and fractional vegetation cover to solve a fourth-order polynomial equation that yields available surface soil moisture. This was then used to create a map of the surface soil moisture distribution. The prevalence of filariasis for each of 173 villages in the southern Nile delta was then compared to an averaged soil surface moisture availability for all of the villages, yielding a relationship between this and the prevalence of filariasis.

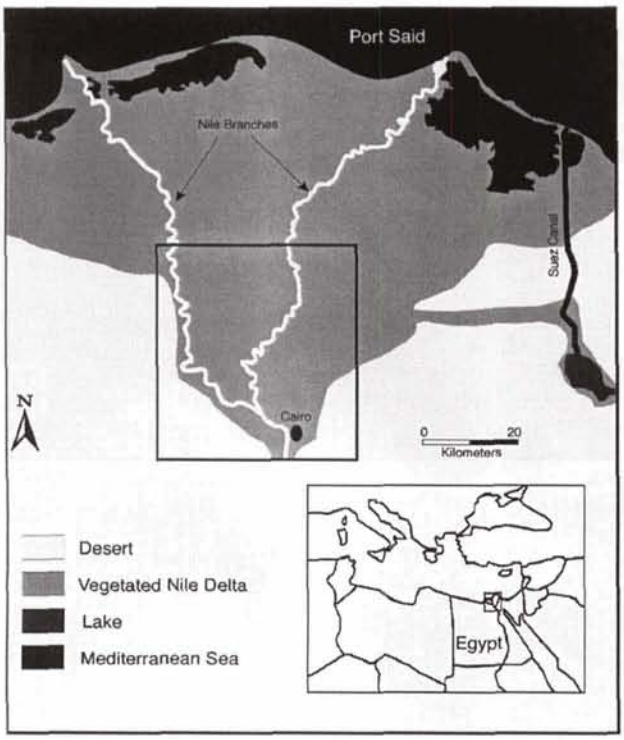

Figure 1. Sketch map of the Nile delta, with the southern Nile delta study area identified within the box. The lagoons at the north of the delta (i.e., Bahra el Manzals, Burullus, and Idku) are easily identifiable.

Analyses such as the one described in this paper have the potential to be useful to local and national governments for identifying regions with environmental risk factors for filariasis, allowing areas of highest risk to be targeted.

Description of Life-Cycle of Filariasis Infection

Bancroftian filariasis is a deforming parasitic infection transmitted by a mosquito vector and caused by the parasite Wuchereria bancrofti. Adult Wuchereria bancrofti are thread-like creamy white worms approximately 8 to 10 cm in length that live in the lymphatic system of the human host for as long as 5 years (Neva and Brown, 1994). Filarial worms cause a complex set of acute and chronic clinical manifestations in humans. Patients with acute filariasis (filarial fever or adenolymphangitis, which may be caused by the host's reaction to dying adult worms in lymphatics) have pain and inflammation over lymphatics draining the legs or male genitalia with fever and general body aches. Chronic filariasis (caused by lymphatic obstruction) includes the classic findings of lymphedema and elephantiasis of the extremities and hydroceles.

Adult female filarial worms give birth to microfilariae, small larvae that circulate in the blood of the human host. During the day the microfilariae are concentrated in the small blood vessels of the lungs. At night the microfilariae make their way to the peripheral blood vessels, which increases the likelihood of ingestion by the vector mosquito (Neva and Brown, 1994).

Transmission of filariasis is dependent on the prevalence of filariasis in humans (a source of infection) and competent vectors, i.e., availability of mosquitoes capable of transmitting the infection (WHO, 1992). The specific mechanism of filariasis transmission involves mosquitoes ingesting microfilariae with blood as they feed on humans. The microfilariae develop in mosquitoes, molting twice over a two-week period to become third-stage infective larvae (L_3) capable of establishing new infections in humans (Sasa, 1976). L_3 are deposited by mosquitoes on the surface of human skin in a small droplet of haemolymph (invertebrate circulatory fluid) when the mosquitoes feed. The L_3 must then make their way to the bite wound, penetrate the bite, and enter the human host (Lindsay *et al.*, 1984). The success of transmission is thought to be dependent on how many infected mosquitoes feed on a host, the loss of the larvae from the mosquito, and penetration of larvae into the host (Lindsay *et al.*, 1984).

In relatively dry regions like Egypt, moisture is probably the single most important environmental factor determining the distribution and spread of mosquito-borne diseases such as filariasis. Mosquitoes require water for breeding and humidity for the prolonged survival (at least 2 weeks) necessary for maturation of filarial larvae to the infective stage (Neva and Brown, 1994). Humidity also affects filariasis transmission. In low-humidity conditions, rapid evaporation of the haemolymph droplet on the skin will decrease the likelihood that the L_3 will enter the human host. The L_3 in the droplet will survive longer under humid conditions, favoring transmission (Lindsay *et al.*, 1984). Thus, overall humidity is a crucial environmental factor in the transmission and regional distribution of filariasis.

Methodology

Determination of Filariasis Prevalence

To better understand filariasis distribution and prevalence in villages in the Nile delta, the Egyptian Ministry of Health conducted filariasis prevalence studies on 314 villages during the period 1985 to 1991 (Harb *et al.*, 1993). One-hundred seventy-three of the villages surveyed fall into the southern Nile delta study area considered in this paper (Plate 1). Approximately 10 percent of the households in the 173 villages (ranging in population from 300 to about 43,000) were tested for filariasis infection. Filarial infections were detected by microscopic

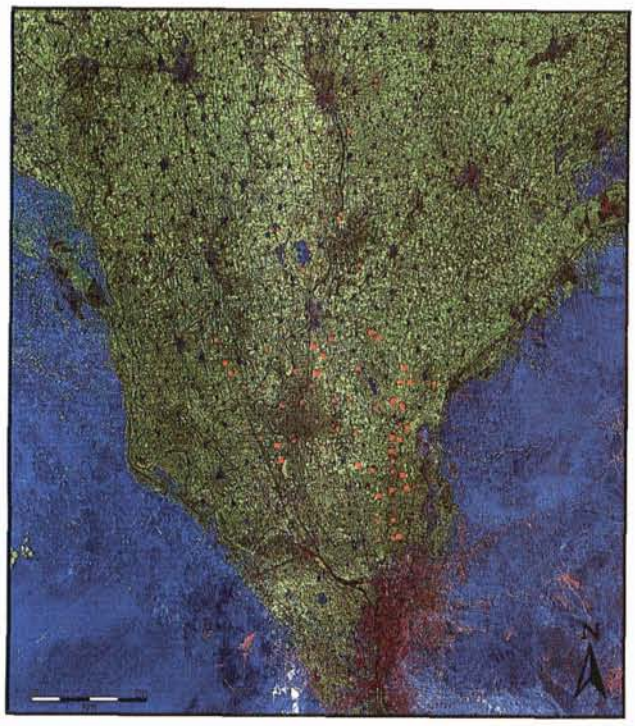

Plate 1. Landsat TM false color composite (bands 2, 4, and 7 as blue, green, red) of the southern Nile delta study area. Blue areas correspond to water and desert, and green areas correspond to vegetated areas. Villages considered in this study are marked in red, with increasing size of the symbol indicating a higher level of infection.

examination of stained thick blood films (20-μl blood samples collected at night) for the presence of microfilariae. Filariasis prevalence in the study area ranged from a low of 0 percent infected to a high of 37.1 percent. It should be noted that filarial infections are chronic, and prevalence rates were probably fairly stable in the Nile delta for the period under study. Prevalence rates do not change by season, and it is therefore reasonable to use the satellite images from 1990 together with infection prevalence data for 1985 through 1991.

Landsat TM Measurements—Data Reduction and Derivation

As stated earlier, in dry regions such as Egypt, humidity may be the single most important environmental factor influencing the distribution of filariasis because humidity is necessary for both transmission of the disease and for maintaining breeding sites for the mosquito vector. Thus, remotely sensed climatologically derived parameters provide an efficient way to examine the regional variability in climatology over the Nile delta.

Landsat TM data acquired for 03 August 1990 (Landsat 4) and 04 August 1990 (Landsat 5) over the southern Nile delta were used to model available surface soil moisture. Two different satellites were necessary because neither encompassed the entire study area. Full-scene products were obtained from Space Imaging EOSAT. All scenes were acquired registered to the Space Oblique Mercator projection and, as a result, arrived resampled (using a nearest-neighbor algorithm) in all bands at a pixel resolution of 28.5 meters.

The available surface soil moisture calculation involves several steps. First, the data were converted to radiance values and then, depending on the band, to surface reflectance or surface radiant temperature. Second, the reflectance data were used to calculate the normalized difference vegetation index (NDVI), which was then converted to normalized NDVI (N^*) and, ultimately, to fractional vegetation cover (Fr). Finally, a normalized temperature ($\hat{T}$) and the fractional vegetation cover were used as the input parameters to solve a fourth-order polynomial equation that yields available surface soil moisture (M_0). This final surface moisture availability field was averaged ($\overline{M}_0$) over a 5-km radius extending from the border of each village. The sections that follow highlight the sequence in which the remotely sensed data were processed. For the sake of clarity, details concerning the scientific basis for the interpretation of the remotely sensed fields of surface reflectance and surface radiant temperature and subsequent numerical reduction to Fr and M_0 are left to the appendix.

Conversion of Digital Numbers to Reflectance and Surface Radiant Temperature

Landsat TM is a passive remote sensing radiometer that records surface brightness values as 8-bit quantization digital numbers (DNs) in seven spectral bands from 0.45 to 12.5 μm. The soil moisture modeling requires Landsat TM band 3 (0.63 to 0.69 μm) in the red wavelengths, band 4 (0.76 to 0.90 μm) in the near-infrared wavelengths, and band 6 (10.4 to 12.5 μm) in the thermal infrared.

Surface Reflectance

Digital numbers for Landsat TM bands 3 and 4 must be converted to values of reflectance to be useful in the calculation of the normalized difference vegetation index which is used for modeling of surface soil moisture. The DNs were first converted to at-sensor Radiance ($mWcm^{-2}sr^{-1}\mu m^{-1}$) using

$$\text{Radiance} = \text{DN} \times \text{Gain} + \text{Bias} \tag{1}$$

where respective Gains ($mWcm^{-2}sr^{-1}\mu m^{-1}$) and Biases ($mWcm^{-2}sr^{-1}\mu m^{-1}$) for bands 3 and 4 are supplied in the Landsat TM header record, or can be calculated from the information supplied by Space Imaging EOSAT. Radiance in bands 3 and 4 was then converted to at-sensor reflectance (Markam and Barker, 1986): i.e.,

$$a = \frac{\pi \cdot \text{Radiance} \cdot d^2}{\varepsilon \cdot \cos z} \tag{2}$$

where a equals reflectance, π is the universal constant, ε is the exoatmospheric irradiance ($mWcm^{-2}\mu m^{-1}$) as specified in EOSAT's technical notes, z is the solar zenith angle (equal to $(90 - \beta)$ or sin β, where β is the solar elevation angle as listed in the Landsat TM header file), and Radiance is as calculated from Equation 1 for respective bands 3 and 4 of the Landsat TM sensor. The parameter d (the Earth-Sun distance) is often omitted from this equation because it is very close to one (1.028, in astronomical units).

Surface Radiant Temperature

Surface radiant temperature was derived from Landsat TM band 6. The calculation of the surface radiant temperature was as follows: The raw band 6 DNs were first calibrated to radiance using Equation 1. The radiometric gains and biases for band 6 were calculated using the algorithm given in the technical information section of Space Imaging EOSAT, as the values supplied in the Landsat TM header file were inaccurate by one decimal place. Radiance (L_6) was then converted to an equivalent blackbody temperature at the satellite using an inversion formula (Singh *et al.*, 1988) of the Planck equation: i.e.,

$$\text{TBB} = \frac{K_2}{K_1 - \ln L_6} \tag{3}$$

where TBB is the equivalent blackbody temperature (K) and, K_2

($mWcm^{-2}sr^{-1}\mu m^{-1}K$) and K_1 ($mWcm^{-2}sr^{-1}\mu m^{-1}$) were assigned values on the basis of discrete intervals in radiant temperature. Appropriate values for K_2 and K_1 are tabulated in Table 1 for Landsat 4 and 5, respectively.

To account for atmospheric effects and so, determine the surface radiant temperature (T_0), the approach of Richter (1996) was used. This approach uses two ground surface temperatures (TS_1 and TS_2) for which corresponding at-satellite blackbody temperatures (TBB_1 and TBB_2) are calculated (assuming a fixed surface emissivity of 0.98). T_0 corresponding to TBB (from Equation 3) was then obtained from linear interpolation of Equation 4: i.e.,

$$T_0 = TS_1 + \frac{TS_2 - TS_1}{TBB_2 - TBB_1}(TBB - TBB_1). \quad (4)$$

The target spots (TS_1 and TS_2) with known temperature, as recorded by Shahin (1985), were located in the Nile river. The first target spot (TS_1) was located in the main channel of the Nile just north of Cairo near the town of Tanash at approximately 30° 07′ 00″N, 31° 13′ 00″E. The second target spot (TS_2) was located at the confluence of the two Nile Channels at approximately 30° 07′ 30″N, 31° 08′ 30″E. The climatological water temperatures recorded for both locations were 20°C (293K).

Derivation of NDVI, Fractional Vegetation Cover, and Surface Moisture Availability

NDVI

Spectral ratios like NDVI make use of the characteristic absorption and reflectance peaks in the vegetation spectrum (i.e., plants absorb highly in the visible wavelengths and reflect highly in the near infrared wavelengths). Accordingly, high NDVI values (large positive fraction) are indicative of densely vegetated surfaces, whereas low NDVI values indicate sparse to no vegetation.

NDVI is, therefore, defined by differencing and ratioing TM bands 3 and 4 of the Landsat TM sensor as follows:

$$NDVI = \frac{(a_4 - a_3)}{(a_4 + a_3)} \quad (5)$$

where a_3 and a_4 are the reflectance values calculated from the measured radiance values in bands 3 and 4 of the Landsat TM sensor.

Strictly speaking, NDVI is defined in terms of surface reflectance (ρ) values for which Equation 2 is corrected to take account of atmospheric effects. Although a number of potential methods for this atmospheric calibration exist, they require specification of atmospheric properties such as aerosols. The limitation here, however, is that the makeup of the atmosphere is inadequately characterized with respect to such properties. To account for any atmospheric variations over the Nile delta, a normalization approach (Equation 6) was applied.

FRACTIONAL VEGETATION COVER

Vegetation biomass (as expressed by the leaf area index (LAI) is highly correlated with NDVI until the former reaches a value of approximately 3 (Baret and Guyot, 1991). Fractional vegetation cover (Fr) is highly correlated with vegetation biomass so that, below a LAI of 3, NDVI will constitute an independent measure of Fr.

The relationship between Fr and NDVI was determined as follows: First, NDVI was scaled between its fully vegetated (maximum NDVI) and bare soil (minimum NDVI) values, creating a re-scaled NDVI or N^* where

$$N^* = \frac{NDVI - NDVI_0}{NDVI_s - NDVI_0} \quad (6)$$

in which $NDVI_s$ and $NDVI_0$ are respectively prescribed (see Appendix) as maximum and minimum values of NDVI. Fr (Equation 7) is then simply expressed as a square function of N^*: i.e.,

$$Fr = N^{*2}. \quad (7)$$

SURFACE SOIL MOISTURE AVAILABILITY[1]

The surface soil moisture availability (M_0) was determined as a fourth-order polynomial equation (Equation 8) which expresses M_0 in terms of Fr and a scaled temperature T: i.e.,

$$M_0 = \sum_{i=0}^{3}\sum_{j=0}^{3} a_{ij}\,\hat{T}^i\,Fr^j \quad (8)$$

The coefficients for the polynomial are given in Table 2. $\hat{T}$ is expressed as

$$\hat{T} = \frac{T_0 - T_0\,(Fr = 1, M_0 = 1)}{T_0(Fr = 0, M_0 = 0) - T_0(Fr = 1, M_0 = 1)} \quad (9)$$

The surface radiant temperature (T_0) was scaled (normalized) between its maximum and minimum values. The purpose behind this normalization is to reduce atmospheric variations between multiple images of different areas acquired at different times. Such a relative calibration of the image data means that a polynomial expression (Table 2) derived for an area in Pennsylvania (Figure 2) can theoretically be applied in a completely disparate location like the Nile delta of Egypt. The extent to which this expression is successful in mapping the NDVI/T_0 domain for the Nile delta is evident by examination of Figure 4a.

Average Surface Soil Moisture Availability

To examine the relationship between available surface soil moisture and prevalence of filariasis, an average surface moisture availability ($\overline{M_0}$) was calculated for a 5-km buffer zone surrounding each village for each of the 173 villages with known prevalence of filariasis. The 5-kilometer radius was chosen to delineate the buffer zone to correspond to a conservative estimation of the flight range of adult female mosquitoes (Horsfall,

TABLE 1. COEFFICIENTS K_1 AND K_2 USED IN THE CALCULATION OF EQUIVALENT BLACKBODY TEMPERATURE IN EQUATION 3

Temperature Range (K)	Landsat-4 TM		Landsat-5 TM	
	K_1	K_2	K_1	K_2
260–300	4.3089	1308.510	4.1754	1274.674
300–340	4.3467	1319.859	4.2171	1287.197

[1]The definition of this variable is given in the appendix.

TABLE 2. POLYNOMIAL COEFFICIENTS FOR POLYNOMIAL EXPRESSION FOR M_0. COURTESY OF CAPEHART (1996).

$$M_0 = \sum_{i=0}^{3}\sum_{j=0}^{3} a_{ij}\hat{T}^i Fr^j, \qquad r^2 = 0.9995, \text{ RMSE} = 0.0069$$

a_{ij}	$j = 0$	$j = 1$	$j = 2$	$j = 3$
$i = 0$	2.5661	−2.0602	0.7707	−0.3062
$i = 1$	−7.7404	−0.3920	−2.8252	−0.2436
$i = 2$	8.5222	7.5239	13.5438	9.2252
$i = 3$	−3.3493	−6.1453	−8.1908	−30.0037

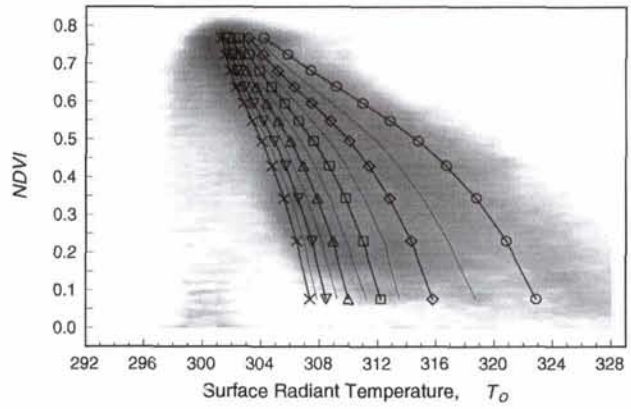

Figure 2. NS001-TMS (Thematic Mapper Simulator) derived T_0-NDVI scatterplot (gray spectral scaling) at a 5-meter spatial resolution for a 7- by 3-km area of the Mahantango Watershed, Pennsylvania, 18 July 1990, 11:45 LST. Isopleths representing moisture availability index, M_0 are overlaid with the legend, o = 0.0 ("warm" edge), ◇ = 0.2, □ = 0.4, △ = 0.6, ▽ = 0.8, and x = 1.0 ("cold" edge). Figure courtesy of Capehart (1996).

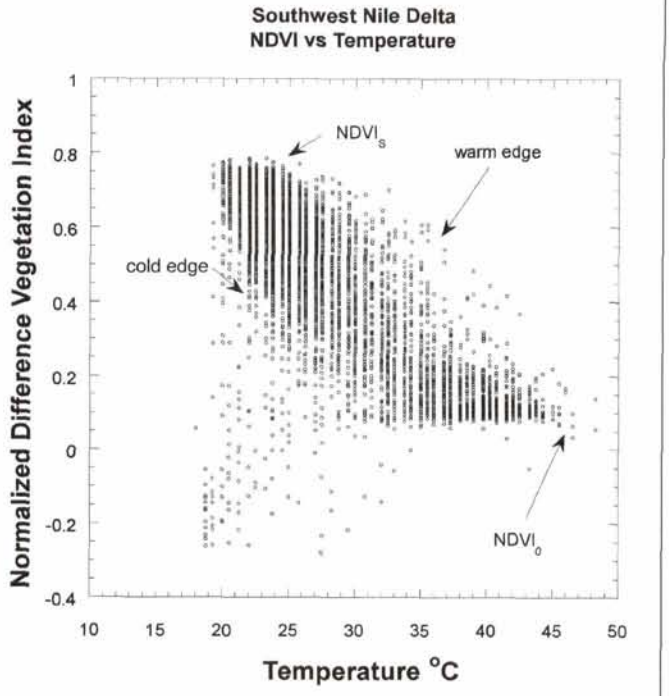

Figure 3. Landsat TM derived T_0-NDVI scatterplot taken over the Nile delta—the equivalent lower resolution plot to Figure 2. The roughly triangular shape of the data is bounded by a clearly delineated "warm" edge, identified with an arrow, on the high temperature edge of the data. Pixels along the "warm" edge are the pixels with highest temperatures and the lowest soil moisture. The "cold" edge is also clearly delineated in this figure and is labeled accordingly. $NDVI_0$, the bare soil NDVI value, is located along the warm edge at the highest observed radiant temperature and minimum NDVI. $NDVI_s$, the 100 percent vegetation cover NDVI value, is located at the point at NDVI ≈ 0.8 where the warm edge begins to bend horizontally. Pixels with negative values of NDVI represent either standing water, clouds, or cloud contamination.

1955). This was done by locating the village of interest in the composite Landsat TM scene, and determining the location of the edges of the village. The village edge was defined as the radius around the village where three-quarters of the image pixels had an *Fr* of less than 0.1; this is a reasonable assumption because the villages are known to have little or no vegetation at the scale of the Landsat TM resampled pixel (28.5 meters). $\overline{M}_0$ for the 5-km border for the buffer zone was then calculated from M_0 values taken from the 175 pixels adjacent to each of the village edge pixels, then averaged around the village to encompass its full areal extent. $\overline{M}_0$ of the 5-km border area surrounding the villages was used as the diagnostic quantity for comparison with the village filariasis prevalence of infection.

Results

Figure 3 is a plot of NDVI versus T_0 for a subset of pixels that include the study area. The feature space is delineated with the characteristics ($NDVI_0$, $NDVI_s$, warm and cold edges) commensurate with the theory (see Appendix). *A priori* knowledge of these key variables permits one to transform the data to N^* and $\hat{T}$ (respectively, Equations 6 and 9) and finally into derived values of *Fr* and M_0 (Equations 7 and 8). Figures 4a and 4b are simply the plotted result of such transformations. While such figures are of little intrinsic use, they provide a graphical context in which to visualize the data with the mathematical transformations applied and overlaid. It also confirms that the data lie within the domain described by the mathematics. Systematic application of these functions (Equations 7 and 8) over the spatial domain (i.e., Nile delta study area) was used to translate the image data into maps of *Fr* and M_0.

Fractional Vegetation Cover

A map of *Fr* for the study area was generated using Equation 7 but because it is comparable to the original TM image (Plate 1), it is not presented here. In general, though, it delineates more visibly those villages surrounded by agricultural areas under various degrees of cultivation. The central portion of the delta appears to have lower *Fr* than either the eastern or western portions of the delta, and the northwestern region has the highest *Fr*. The *Fr* map provides an indication of the irrigated areas where there exists sufficient rooting zone water content to render plant growth and support varying degrees of cultivation.

Surface Soil Moisture Availability

The surface soil moisture availability (M_0) polynomial (Equation 8) was used to create a surface soil moisture availability map for the southern Nile delta (Plate 2A). In general, the south-central portion of the delta has very high M_0. The southeastern delta is generally wetter than the northwestern section of the delta, although the northwestern section has a greater *Fr*. Plate 2B is a full resolution image (i.e., all pixels displayed) of a village (outlined in white) surrounded by an area with high M_0. This village had a relatively high prevalence of filariasis infection. Plate 2C is a full resolution image of a village (outlined in white) surrounded by an area with low M_0 and had a low prevalence of filariasis infection.

Comparison of Filariasis Prevalence and Averaged Surface Soil Moisture Availability

A scatterplot of filariasis prevalence versus $\overline{M}_0$ (Figure 5) shows that filariasis prevalence rates are negligible in villages with $\overline{M}_0$ below 0.2. Villages surrounded by areas of particularly high $\overline{M}_0$

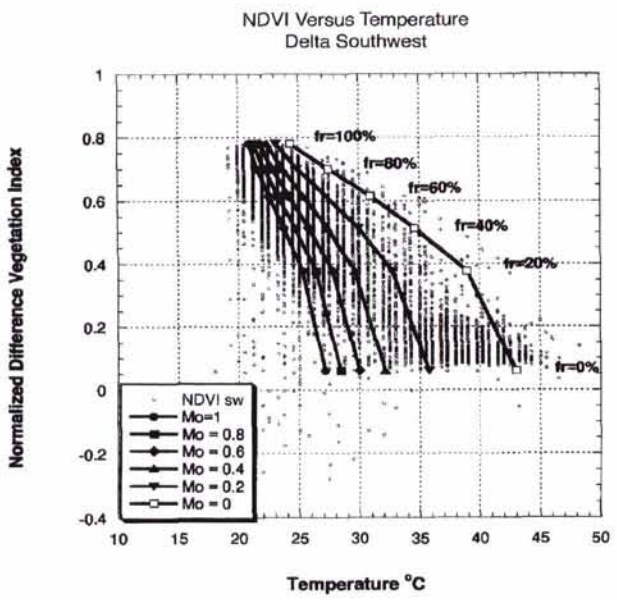

(a)

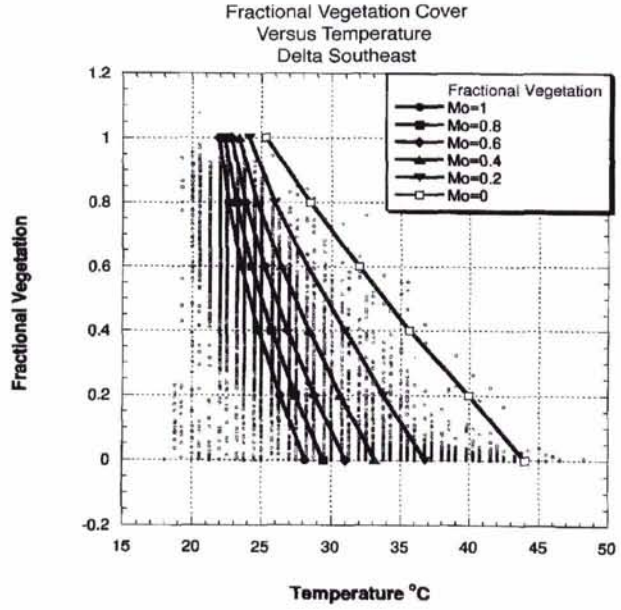

(b)

Figure 4. (a) Plot of NDVI versus surface radiant temperature (T_0) for the Nile delta Southwest. Isopleths of surface soil moisture availability (M_0) overlie the data. Symbols along the M_0 isopleths indicate fractional vegetation cover of between 0 and 100 percent. (b) Same as (a) but with ordinate axis given in terms of *Fr* and superimposed over pixels taken from the Nile delta Southeast. The M_0 isopleths form a triangle and converge at high *Fr*, due to the insensitivity of vegetation temperature to surface soil water content. The upper portion of the M_0 triangle is an area where errors in the M_0 calculation will be greatest.

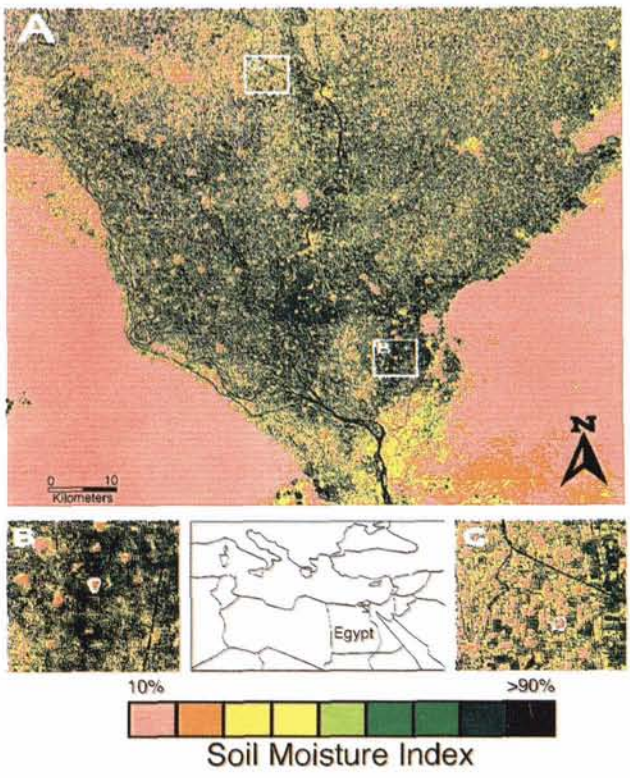

Plate 2. (A) Map of regional surface soil moisture availability (M_0) for the Nile delta study area. Dark colors indicate high soil moisture and light colors indicate low surface soil moisture availability. (B) Full resolution map (28.5-meter pixels) of surface soil moisture availability near the village El-Kashish which has high soil moisture and a high filariasis infection rate. (C) Full resolution (28.5-meter pixels) map of the village El-Aysha, which is surrounded by low surface soil moisture availability and has a low filariasis infection rate.

(0.5 to 0.6) also have low levels of filariasis infection but, because only a few villages lie within this range, the lack of data for these high values precludes significant conclusion. These observations suggest that there is a critical amount of soil moisture necessary for moderate to high rates (greater than 5 percent infection) of filariasis infection. The critical soil moisture value lies above 0.2 $\overline{M}_0$, with the highest prevalence of the disease falling between soil moisture values of 0.3 and 0.44. Villages in areas with soil moisture levels above the apparent threshold value of 0.2 have highly variable infection levels. The linear correlation coefficient (R^2) between filariasis prevalence in the population and $\overline{M}_0$ is 0.37. A partial linear correlation with the effects of the different areas of villages removed is still about 0.37, so the conclusion is that there is only a threshold effect in which moisture below about 0.2 keeps infections way down.

It has been hypothesized that smaller villages in Egypt may be at a greater risk for filariasis compared to larger villages. Mosquito density and biting rates tend to be highest at the periphery of villages, adjacent to agricultural land. Small villages have a relatively greater exposure to the source of mosquitoes than larger areas (i.e., a greater surface area/population or circumference/area ratios). This possibility (i.e., a relationship between village size, filariasis prevalence, and $\overline{M}_0$) was also investigated. The results of the statistical analysis ($R^2 = -0.03$) indicate that village size is not a contributing factor to the prevalence of the infection.

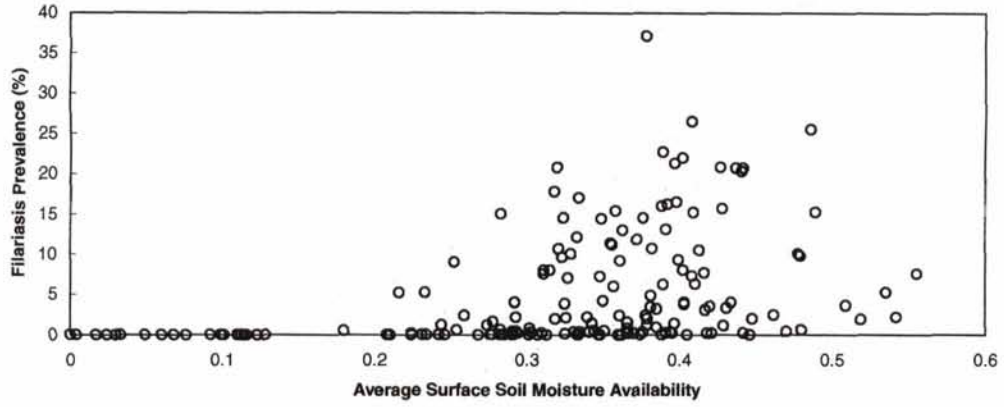

Figure 5. Plot of averaged surface soil moisture availability ($\overline{M}_0$) versus filariasis prevalence. This plot shows that below soil moisture of 0.2 infection rates were negligible. Infection rates were also low in areas with available soil moisture values above 0.5. Infection rates were variable in areas with soil moisture values between 0.2 and 0.5.

Conclusions and Discussion

It is possible that the critical surface soil moisture availability greater than 0.2 $\overline{M}_0$ for high filariasis prevalence reflects habitat conditions most favorable for mosquito breeding and their survival. Low infection prevalence in villages with below 0.2 $\overline{M}_0$ may reflect conditions in which low humidity interferes with mosquito breeding, survival and transmission of L_3 from mosquitoes to humans. The corollary to this, in which high $\overline{M}_0$ (above 0.5) would imply higher ambient atmospheric humidity and resultant higher prevalence of the disease, is not so straightforward. It is feasible that the higher values of $\overline{M}_0$ are indicative of more rigorous irrigation practices that might indicate consistent water usage from the irrigation channels. Such active practices would keep channel water flowing, as well as cause disruptions in the flow of the water. This in turn may well prevent the establishment of stable breeding habitats for the mosquitoes. In addition, Culex pipiens mosquitoes breed in stagnant, polluted water. If surface water in areas of high moisture is cleaner, this could tend to decrease Culex pipiens breeding.

It is interesting to note that villages in areas with soil moisture levels above the apparent threshold value of 0.2 had variable levels of infection. This is at first puzzling, given that inspection of individual cases suggests otherwise—low M_0 indicating low prevalence of the disease and vice-versa. This may be due to a combination of confounding factors, such as pesticide use to decrease mosquito density and survival and the distribution of antifilarial drugs to treat human populations (e.g., diethylcarbamazine), as well as socioeconomic factors associated with seasonal labor migration practices. These practices can certainly affect filariasis prevalence rates. Other factors such as prevailing winds, crop selection, population density of both humans and domestic animals, and local variability of dominant mosquito species and strains could also contribute to the observed variability in infection. Field data sets that could be used to evaluate these parameters were not available to stratify the analysis. Further studies are needed to sort out factors that might contribute to the variability in infection prevalence rates found within the critical soil moisture window.

Overall, it is not apparent that average surface soil moisture, above a threshold value of 0.2 in the vicinity of villages, is a significant environmental indicator of filariasis prevalence and risk in the southern Nile delta. The study identified a range in M_0 that seems to be permissive for filariasis transmission, although prevalence rates in "high-risk" villages are highly variable. While additional studies are needed to establish the predictive value of this method for estimating the risk of filariasis in other areas in Egypt and in other countries, one should be able to use this approach to distinguish high risk villages from villages with little or no risk of filariasis. The method is easily applicable and relatively inexpensive. Thus, remote sensing of soil moisture is a potentially useful tool for filariasis control efforts that is worthy of further study, because it should help health authorities to focus surveillance and control efforts (drug therapy and mosquito control) in high risk areas and thereby take full advantage of scarce resources.

Acknowledgments

Work by Ray E. Arvidson and Kate Crombie was supported in part by Goddard Space Flight Center Grant NAG-5-2982, NASA Solid Earth Sciences and National Hazards Program. The participation by Robert R. Gillies was supported in part by the Utah Agricultural Experiment Station, Utah State University, Logan, Utah. Gary J. Weil's research in Egypt is supported by NIH grant AI35855. The authors are indebted to the reviewers for their suggestions on improving the preliminary manuscript.

References

Baret, F., and G. Guyot, 1991. Potentials and limits of vegetation studies for LAI and PAR assessment, *Remote Sensing of Environment*, 35:161–174.

Beck L.R., M.H. Rodriguez, S.W. Dister, A.D. Rodriguez, E. Rejmankova, A. Ulloa, R.A. Meza, D.R. Roberts, J.K. Paris, M.A. Spanner, R.K. Washino, C. Hacker, and L.J. Legters, 1994. Remote sensing as a landscape epidemiological tool to identify villages at high risk for malaria transmission, *American Journal of Tropical Medicine and Hygiene*, 51(3):271–280.

Capehart, W.J., 1996. *Issues Regarding the Remote Sensing and Modeling of Soil Moisture for Meteorological Applications*, Ph.D. Thesis, Department of Meteorology, The Pennsylvania State University, State College, 238 p.

Capehart, W.J., and T.N. Carlson, 1997. Decoupling of surface and near-surface soil water content: a remote sensing perspective, *Water Resources Research*, 33(6):1383–1395.

Carlson, T.N., and F.E. Boland, 1978. Analysis of urban-rural canopy using a surface heat flux/temperature model, *Journal of Applied Meteorology*, 17:1000–1013.

Carlson, T.N., R.R. Gillies, and E.M. Perry, 1994. A method to make use of thermal infrared temperature and NDVI measurements to infer surface soil water content and fractional vegetation cover, *Remote Sensing Reviews*, 9:161–173.

Carlson, T.N., and D.A.J. Ripley, 1997. On the relationship between NDVI, fractional vegetation cover and leaf area index, *Remote Sensing of Environment*, 62:241–252.

Choudhury, B. J., N.U. Ahmed, S.B. Idso, R.J. Reginato, and C.S.T. Daughtry, 1994. Relationships between evaporation coefficients and vegetation indices studied by model simulations, *Remote Sensing of Environment*, 50:1–17.

Feinsod, F.M., R. Faris, A. Gad, S. El Said, B.A. Soliman, I.S. Abd-El Azem, and A.J. Saah, 1987. Clinical manifestations of Wuchereria bancrofti filariasis in an endemic village in the Nile delta, *Annals de la Societe Belge de Medecine Tropicale*, 67:259–265.

Fisher, L.D., and G. van Belle, 1993. *Biostatistics: A Methodology for the Health Sciences*, John Wiley & Sons, Inc., New York, 991 p.

Gillies, R.R., and T.N. Carlson, 1995. Thermal remote sensing of surface soil water content with partial vegetation cover for incorporation into climate models, *Journal of Applied Meteorology*, 34:745–756.

Gillies, R.R., J. Cui, T.N. Carlson, W.P. Kustas, and K.S. Humes, 1997. Verification of a method for obtaining surface energy fluxes of surface soil moisture availability from remote measurements of NDVI and surface radiometric temperature, *International Journal of Remote Sensing*, 18(15):3145–3166.

Goward, S., G.D. Cruickshanks, and A. Hope, 1985. Observed relation between thermal emission and reflected spectral radiance of a complex vegetated landscape, *Remote Sensing of Environment*, 18:137–146.

Harb, M., R. Faris, A.M. Gad, O.N. Hafez, R. Ramzy, and A.A. Buck, 1993. The resurgence of lymphatic filariasis in the Nile delta, *Bulletin of the World Health Organization*, 71(1):49–54.

Horsfall, W.R., 1955. *Mosquitoes: Their Bionomics and Relation to Disease*, Ronald Press Co., New York, 723 p.

Idso, S.B., T.J. Schmugge, R.D. Jackson, and R.J. Reginato, 1975. The utility of surface temperature measurements for the remote sensing of surface soil water status, *Journal of Geophysical Resources*, 80(21):3044–3049.

Kustas, W.P., and J.M. Norman, 1996. Use of remote sensing for evapotranspiration monitoring over land surfaces, *Hydrological Sciences*, 41(4):495–516.

Lindsay, S.W., D.A. Denham, and P.B. McGreevy, 1984. The effect of humidity on the transmission of Brugia phangi infective larvae to mammalian hosts by Aedes aegypti, *Transactions of the Royal Society of Tropical Medicine and Hygiene*, 78:19–22.

Lynn, B., and T.N. Carlson, 1990. A stomatal resistance model illustrating plant vs. external control of transpiration, *Agricultural and Forest Meteorology*, 52:5–43.

Malone, J.B., O.K. Huh, D.P. Fehler, P.A. Wilson, D.E. Wilensky, R.A. Holmes, and A. El Magdoub, 1994. Temperature data from satellite imagery and the distribution of shistosomiasis in Egypt, *American Journal of Tropical Medicine and Hygiene*, 50(6):714–722.

Malone, J.B., O.K. Huh, M.S. Abdel-Rahman, M.M. El Bahy, O.K. Huh, M. Shafik, and M. Bavia, 1997. Geographic information systems and the distribution of Shistosoma manosoni in the Nile delta, *Parasitology Today*, 13:112–119.

Markam, B.L., and J.L. Barker, 1986. Landsat MSS and TM post-calibration dynamic ranges, exoatmospheric reflectances and at-satellite temperatures, *EOSAT Landsat Tech. Note*, 1:3–8.

Neva, F.A. and H.W. Brown, 1994: *Basic Clinical Parasitology*, Appleton-Century-Crofts, Norwalk, Connecticutt, pp. 152–158.

Ottesen, E.A. and C.P. Ramachandran, 1995. Lymphatic filariasis infection and disease: Control strategies, *Parasitology Today*, 11:129–131.

Price, J.C., 1990. Using spatial context in satellite data to infer regional scale evapotranspiration, *IEEE Transactions on Geoscience and Remote Sensing*, GE-28:940–948.

Richter, R., 1996. A spatially adaptive fast atmospheric correction algorithm, *International Journal of Remote Sensing*, 17(6):1201–1214.

Rodgers, D.J., and S.E. Randolph, 1991. Mortality rates and population density of tsetse flies correlated with satellite imagery, *Nature*, 351:739–741.

Sasa, M., 1976. *Human Filariasis*, Universtiy of Tokyo Press, 48 p.

Shahin, M., 1985. *Hydrology of the Nile Basin*, Elsevier, Amsterdam, 575 p.

Singh, S.M., 1988. Brightness temperature algorithms for Landsat Thematic Mapper data, *Remote Sensing of Environment*, 24:509–512.

Southgate, B.A., 1979. Bancroftian filariasis in Egypt, *Tropical Diseases Bulletin*, 76(12):1047–1668.

Taconet, O., T.N. Carlson, R. Bernard, and D. Vidal-Madjar, 1986. Evaluation of a surface/vegetation parameterization using satellite measurements of surface temperature, *Journal of Applied Meteorology*, 25:1752–1767.

Thompson, D.F., J.B. Malone, A.A. Buck, and B.L. Cline, 1996. Bancroftian filariasis distribution in the southern Nile delta: Correlation with diurnal temperature differences from satellite imagery, *Emerging Infectious Diseases*, 2:234–235.

WHO, 1992. *Fifth Report of the WHO Expert Committee on Filariasis*, WHO Technical Report Series No. 821, World Health Organization, Geneva, 71 p.

Received 02 March 1998; accepted 09 September 1998; revised 14 February 1999

Appendix - The Triangle Method

A physical model (ABL-SVAT[2]) is often used for the interpretation of primary remotely sensed fields, i.e., measurements of surface reflectance and surface radiant temperature. This has the potential to introduce uncertainty in the derived products. The technique described here reduces such uncertainties because it identifies physical limits found in the remotely sensed data which are subsequently used to constrain the solution for obtaining the climatological fields. The generated climatological fields are surface moisture availability (M_o) and fractional vegetation cover (Fr). Sensible heat flux (H), evapotranspiration (ET), and net radiation (RNET) can also be derived.

A technique referred to as the triangle method is a multispectral method which combines measurements of surface radiant temperature (T_o) and reflectance (red and near infrared). The reflectance measurements are used to calculate the Normalized Difference Vegetation Index (NDVI). NDVI is subsequently plotted as a function of T_o, and the observed association between the two variables is illustrated in Figure 2.

The physical limits which constrain the solution for the climatological fields are defined from the scatterplot, of which Figure 2 is a high-resolution example. It relies theoretically upon observing the complete spectrum of Fr and M_o at the ground surface. By definition, then, the observations must be bounded by their physical limits and will manifest themselves as boundaries - visually characterized in the observations by distinct edges.

Such edges for Fr are straightforward, where a low NDVI extreme and a narrow vertex at the high NDVI extreme represent zero (bare soil) to 100 percent (complete canopy) vegetation cover, respectively-this relationship between the NDVI and Fr is non-linear. The edges associated with the limits of M_0 are somewhat more difficult to visualize and describe. This is due to (a) the nature of the spectral plot (Figure 2) which makes it difficult to isolate extraneous pixels (which are relatively few in number) that tend to mask the edge, and (b) the physics which specifies the temperature soil water content (M_0) relationship. Careful observation (with the aid of the model output of M_0) helps delineate (a) whereas, for (b), the work of Idso *et al.* (1975), who describes the physics, is translated by Goward *et al.* (1985), Price (1990), and Carlson *et al.* (1994), who apply the theory to NDVI/T_0 space. The relevant point to come from

[2]ABL-SVAT: Atmospheric Boundary Layer - Soil Vegetation Atmosphere Transfer Model. Carlson and Boland (1978), Taconet *et al.* (1986), and Lynn and Carlson (1990).

their interpretation of the physics is that the warmest pixels (despite variations in *Fr*) correspond to the driest surfaces and define an edge; the so-called "warm" edge that represents a minimum limit of M_0. At the other extreme, the opposite applies where a "cold" edge represents a maximum limit of M_0.

It is evident from theoretical considerations alone that within the domain of the scatterplot there must exist all possible permutations of *Fr* and M_0. The issue then is to map the domain appropriately. This is where the remote observations are coupled to a physically based algorithm (usually a model) and the conceptual interpretation is (climatological fields) the result. A review and categorization of various techniques (for determining evapotranspiration) is given by Kustas and Norman (1997).

Exploiting the NDVI/T_0 Relationship with the Triangle Method

A first step in the process is to establish the relationship between Fr and NDVI. First, NDVI is scaled between its fully vegetated (maximum NDVI) and bare soil (minimum NDVI) values, creating a re-scaled NDVI or N^* where

$$N^* = \frac{\text{NDVI} - \text{NDVI}_0}{\text{NDVI}_s - \text{NDVI}_0} \tag{A1}$$

in which NDVI_s and NDVI_0 are, respectively, the maximum and minimum values of NDVI.

The transform between N^* and *Fr* is obtained by fitting model output to the satellite data along the "warm" edge with M_0 set to zero for two conditions: 100 percent vegetative cover with the maximum NDVI (known *a priori*) and bare soil conditions knowing the minimum NDVI. Using ancillary data (including a morning sounding, vegetation, and soil type information), the model is tuned until the modeled and measured T_0 are closely matched for both cases. The model is subsequently run in increments of fractional vegetation cover so that $T_0 = f(Fr)$. By representing the warm edge as a regression of N^* against T_0, $T_0 = f(Fr)$, the two relationships can be used to associate N^* with *Fr*. Applying this method to satellite data from the Mahantango Creek watershed, Pennsylvania, Konza Prairie, Kansas and Newcastle-on-Tyne, United Kingdom, a simple relationship (Gillies *et al.*, 1997) was derived, where

$$Fr = N^{*2}. \tag{A2}$$

This is similar to a relationship by Choudhury *et al.*, (1994), in which they related the leaf area index to NDVI. Other independent support (radiation transfer calculations) for this simple square root relationship is to be found in Carlson and Ripley (1997). Of further significance, their work suggests that this scaling eliminates errors in the reflectance data that are attributed to sensor calibration and atmospheric correction. With the Fr/N^* relationship, it is a simple matter to transform the remote observations from NDVI/T_0 space to Fr/T_0 space.

The second step is to derive M_0. The same iteration scheme as described earlier for M_0 set to zero is adopted with the exception that M_0 is now also cycled over its theoretical range (i.e., 0 to 1). The output of this process is a matrix of data which assigns the model variable (M_0) to the remote measurements (T_0) but, most importantly, the variable is constrained by the physical limits implied by the remote observations, as evidenced by the M_0 overlay in Figure 2. This matrix can be expanded to include model derived sensible heat (H) and evapotranspiration (ET) - which are model output variables. The only step left in the process it to mathematically derive the coefficients necessary to fit the data, for example ET = $f(Fr, M_0)$. A further modification to the technique uses a scaled temperature for both the model and remotely sensed values of T_0. Similar to N^*, this scaled temperature, $\hat{T}$, is expressed as

$$\hat{T} = \frac{T_0 - \overline{T}_0(Fr = 1, M_0 = 1)}{T_0(Fr = 0, M_0 = 0) - T_0(Fr = 1, M_0 = 1)} \tag{A3}$$

so that the temperature, like NDVI is scaled between its maximum and minimum values. Unlike the case for the NDVI, this scaling reduces, though it does not eliminate, calibration and correction issues. This is referred to as the "stretched triangle." One final point to be made at this time is that, because of errors inherent in calculating T_0, and because the triangle narrows along the temperature axis, the usable area of the triangle domain is below 80 percent *Fr*.

Further Explanation and Information about *Fr* and M_0

Fractional Vegetation Cover (Fr)

The derivation of *Fr* is described in the previous section. Though *Fr* is exclusively a function of NDVI, the extremes of NDVI used to calculate N^* require information taken from the scatterplot. In the event that a scatterplot is not complete, a value for NDVI_0 can be extracted from neighboring urban pixels. In cases where the NDVI is not expected to represent 100 percent vegetation in a given scene, the value of NDVI_s can be approximated by extrapolating a polynomial representation of the "warm" edge in T_0/NDVI space into a T_0 commensurate with the ambient air temperature. Then, a working value of NDVI_s can be estimated.

Moisture Availability Index (M_0)

The surface soil moisture availability (M_0) is also related to the surface soil water content. For bare soil, M_0 is based on a ratio of the surface soil water content to its value at field capacity above which the soil water evaporates at the potential rate. For a vegetation canopy, M_0 continues to refer to the soil below the canopy. Soil water from vegetation itself is extracted from the lower of the ABL-SVAT's two soil layers. Validation of the triangle method was conducted by Gillies *et al.* (1997) where good agreement was found between the gravimetric measurements and NS001 derived estimates obtained from FIFE and Walnut Gulch, Arizona. However, linking tangible estimates of soil water content from AVHRR data has been shown to be problematic due to the high spatial variability of the surface soil moisture, especially under drying conditions (Capehart and Carlson, 1997). At such coarse resolution, thermally derived M_0 may have little physical meaning beyond that of an index.